Colloid & Polymer Science Colloid Polym Sci 272:755–769 (1994)

Original Contributions

Acrylic acid copolymer nanoparticles for drug delivery: structural characterization of nanoparticles by small-angle x-ray scattering

J. J. Müller[1]*, G. Lukowski[2]*, R. Kröber[1], G. Damaschun[1], and M. Dittgen[3]

[1] Max-Delbrück-Centre for Molecular Medicine, Berlin-Buch
[2] Department of Pharmaceutics, E.-M.-Arndt-University, Greifswald
[3] Jenapharm GmbH, Jena, FRG

Abstract: Nanoparticles are possible carriers for drug delivery. Copolymer nanoparticles of acrylic acid, acrylic amide, acrylic butylester, and methacrylic methylester (CAA) dispersed in water and in 0.15 M NaCl-solution were investigated by small-angle x-ray scattering (SAXS) experiments. The particles were characterized in terms of parameters relevant for the in vivo distribution: particle shape and diameter, size distribution, surface structure, and their organization within tight systems.

The CAA-nanoparticles exist in at least three populations of spheres with two minor subpopulations having radii of about 32 and 66 nm and the main moiety around 45 nm. The degree of polydispersity is $R_w/R_N = 1.05$. The subpopulations possess different hydrophobic areas on their surfaces, leading to different recognition by opsonins in vivo and different organ distribution and clearance velocity. The particles are compact without channels and holes, which is proved by low internal hydration $w = 0.22$ g H_2O/g polymer. Drugs and coating surfactants will interact mainly with the outer surface and not tunnel into the carriers. The surface of the nanoparticles is fractal with a dimension $D = 2.3$. Probe-molecules with dimensions less than 11.4 nm in diameter will find a larger contact area than expected from the sphere radius. Adsorption rate and position of the arrival of surfactants, and possibly opsonins, may be affected thereby. The negative charges on the CAA-nanoparticle surface are nearly completely screened in physiological NaCl-solutions by counter-ions. Therefore, surface charges hamper carrier-cell interaction at short distances only and do not prevent specific recognition and clearance by the reticuloendothelial system (RES).

Key words: Small-angle x-ray scattering (SAXS) – nanoparticles – acrylic acid copolymer – fractal surface

Introduction

The effective use of pharmacological active substances in the chemotherapy of cancer, viral infections, and many other pathological processes suffers from non specific toxicity and poor tissue specifity of the drugs. Specific targeting of pharmaca can increase their effectiveness in the target tissue and reduce general toxicity. Polymeric nanoparticles are possible carriers for such controlled drug delivery and targeting by an intravenous route [1, 2]. Many biochemical and biophysical parameters affect the distribution of the polymeric particles in vivo, such as particle charge [3], surface hydrophobicity [4, 5], particle diameter [6], particle shape and surface structure features [7]. Particles with high hydrophobicity or charge are more rapidly cleared than less

* to whom correspondence should be addressed

hydrophobic and non-charged ones. The uptake of carriers by the liver and spleen increased when the particle size increased. The adsorption of opsonins, which influence the recognition by the reticuloendothelial system (RES), depends also on surface hydrophobicity, charges, surface structure and the shape of the particles. Furthermore, these parameters are essential for understanding binding processes of surfactants and drugs at the surface of nanoparticles [8].

Model carriers containing acrylic acid, acrylic amide, acrylic butylester, and methacrylic methylester were produced [9]. The surface hydrophilicity can be altered by varying the monomer ratios in the copolymers. An increase of the acrylic acid content in copolymers reduces the surface hydrophobicity of nanoparticles distinctly [9]. The aim of the small-angle x-ray scattering (SAXS) experiments discussed in this paper is a more detailed physical characterization of the most hydrophilic nanoparticles from a series corresponding to their shape, diameter, diameter distribution, surface structure, and their organization in tight systems under different ionic conditions. The results are the basis for further biophysical investigations of coated carriers loaded with drugs and macromolecules.

Experimental

Materials

Different copolymer particles of acrylic acid (CAA) with acrylic amide, acrylic butylester, and methacrylic methylester were produced by emulsion polymerization in water as previously described [9]. The most hydrophilic polymer is composed from 14.4% acrylic acid, 56.0% methacrylic methylester, 3% acrylic amide, and 26.6% acrylic butylester.

The CAA-particles were getting out as a latex of about 50% in solid phase. The latex sample was purified by dialysis against double distilled water in open air. The ion concentration should then correspond to 10^{-3}–10^{-4} M in the sample, as described by Ametani and Fujita [10]. The polymer concentrations used for small-angle experiments are 1.36, 2.26, 4.65, 8.9, 17.9, and 39.5 mg/ml.

A second series (CAA-NaCl) was measured in a physiological sodium chloride-solution (0.15 M NaCl) with polymer concentrations of 4.41, 8.57, 17.27, and 34.5 mg/ml. NaCl was purchased from Sigma.

The samples were investigated at room temperature by small-angle x-ray scattering experiments in thin-walled glass-capillaries 1 mm in diameter.

Methods

Small-angle x-ray scattering experiments

The measurement of the small-angle x-ray scattering intensity was done by using a Kratky diffractometer (A. Paar KG, Graz) with electronic step scanner and data acquisition by a personal computer. The scattered Cu-K_α-radiation was registered by a proportional counter after monochromatization by a 7 μm Ni-filter and pulse height discrimination. Widths and positions of the entrance and of the receiving slits guarantees a loss-free registration of information of the scattered intensity for scattering vectors larger than $s_{min} = 0.012\ nm^{-1}$. This therefore provides structure information up to dimensions of 260 nm [11]. $s = 4\pi \sin \Theta/\lambda$ is the length of the scattering vector, with the wave length λ and the scattering angle 2Θ. The upper limit of the scattering vector was $s_{max} = 0.52\ nm^{-1}$. A structure resolution of the experiments of about 6 nm results from this.

The data correction of slit width and slit length smearing effects caused by the diffractometer geometry was done by direct methods combined in the FORTRAN program-system SAXS 1.0 running on an IBM-PC [12]. The data evaluation procedures concerning removement of aggregates, extrapolation to infinite polymer dilution, particle size distribution, model fitting [13], molecular mass determination, fractal analysis, and the simulation of densely packed systems are also included in the program package.

Theory

The theoretical background of the small-angle x-ray scattering and the data handling and evaluation has been described recently in two textbooks [14, 15].

Here, we will only refer to the newer methods for calculating the particle distribution function, for determining the molecular mass, and for determining functions describing the nanoparticle solution structure.

Particle size distribution function

For a polydisperse system of spheres the scattered intensity is given by

$$I(s) = \int_{L_{min}}^{L_{max}} N(D) \cdot I_D(s, D) dD \,. \tag{1}$$

L_{max} is the diameter D of the largest particle and L_{min} that of the smallest. $N(D)$ is the number distribution when $I(0, D) \sim V^2(D)$, which is the squared volume of the particles with the diameter D. Following the algorithm proposed by Walter et al. [16], the number distribution can be calculated directly via

$$N(D) = -\frac{d}{dx}(C''(x)/x)_{x=D} \tag{2}$$

from the scattered intensity $I(s)$ at discrete points $k \cdot \Delta s$:

$$N(D) = \frac{\Delta s^2}{2 \cdot \pi^2} \sum_{k=0}^{M} k \cdot I(k \cdot \Delta s) \left\{ \sin(k \cdot \Delta s \cdot D) \cdot \left[\frac{8}{D^5} - 4(k \cdot \Delta s)^2 / D^3 \right] + \cos(k \cdot \Delta s \cdot D) \left[\frac{(k \cdot \Delta s)^3}{D^2} - \frac{8k \cdot \Delta s}{D^4} \right] \right\} + R_i \tag{3}$$

($C(x)$-spherically averaged autocorrelation function of the particles).

R_i is a correction term taking into account a tail extrapolation of the scattering curve by c_1/s^3 or c_2/s^4 for termination error reduction.

For a c_1/s^3–tail holds

$$R_1(D, q) = \frac{c_1}{2\pi^2} \left[\sin qD \cdot \left[\frac{8}{qD^5} - \frac{q}{D^3} \right] - \frac{5}{D^4} \cos qD \right], \tag{4}$$

and for a c_2/s^4–tail

$$R_2(D, q) = \frac{c_2}{2\pi^2} \left[\sin qD \cdot \left[\frac{4}{q^2 D^5} - \frac{1}{D^3} \right] - \frac{4}{qD^4} \cos qD \right], \tag{5}$$

with $q = s_{start} + \Delta s/2$, where s_{start} is the first scattering vector within the tail and Δs is the step width.

A proof of the relevance of the directly calculated distribution function $N(D)$ can be realized by digitizing $N(D)$ and rewriting Eq. (1) for a discontinuous function

$$I_{rec}(s) = \sum_{i=L_{min}/\Delta x}^{L_{max}/\Delta x} N(i \cdot \Delta x) \cdot I(s, i \cdot \Delta x) \,, \tag{6}$$

where Δx is the width of the interval for the step function $N(i \cdot \Delta x)$.

Molecular mass determination

If a direct measurement of the scattered intensity in absolute units via a standard sample [17, 18] is extremely difficult, e.g., because of a high-resolution slit configuration of the diffractometer and therefore lacking intensity, the method recently developed by Plestil et al. [19] is the method of choice for the determination of molecular masses. The weight average of the molecular mass is calculated from

$$M_w = \frac{N_L [I(0)/c]_{c=0}}{-\frac{dz}{dc}} \,, \tag{7}$$

with the reduced Porod's invariant

$$z = \frac{1}{2\pi^2} \int_0^\infty \frac{I(s, c)}{c} s^2 ds \,. \tag{8}$$

The prerequisite is that the reduced scattered energy z must depend on the concentration c of the particles.

Then, the first derivative dz/dc differs from zero, and the weight average of the molecular mass can be calculated from a series of measurements of scattering curves at different concentrations. The scattered intensity at zero angle and for zero concentration has to be estimated in the same way as for the molecular mass determination using absolute scattered intensities [14]. Sometimes the method fails, as has been discussed critically by the authors themselves [19], and as will be shown later on.

Interparticular scattering effects

Shape and particle dimensions, as well as a particle size distribution, can be determined if correlations between the orientation or positions of the particles in solution are negligible. This

precondition is usually reached by measuring a concentration series and quasilinear extrapolation of the scattered intensity to zero concentration [14]. For higher concentrations or for charged particles, long-range interactions have to be taken into account. General principles for the analysis of scattering data of more closely packed particles have been given by Guinier et al. [20] and Enderby and March [21]. Palmer and Weeks [22], Hayter and Penfold [23], and Hansen and Hayter [24] took into account Coulomb repulsion between spherical particles and derived structure factors for such solutions. In the spherical approximation the scattering can be factorized in

$$I(s, c) = N \cdot I_p(s) \cdot a(s, c) , \quad (9)$$

where N is the number of molecules in the sample which is proportional to the concentration c. An exact simulation as well as an experimental determination of the interaction term $a(s, c)$ is difficult, especially for charged particles. The form factor of the independent scattering of single particles $I_p(s)$ has to be determined in the infinite dilution approximation, e.g., for infinite small concentrations of the macromolecule in an excess-salt regime. The last condition may lead to formation of aggregates, in which scattering disturbs the particle form factor measurement. For a system of particles with Lenard-Jones interaction potentials and showing impenetrability and form constancy (hard spheres), the solution structure factor was derived by Fournet [25] to be

$$a(s, c) = \frac{1}{1 + 8\mu \cdot \Phi(2Rs)} . \quad (10)$$

$\Phi(2Rs)$ is the scattering amplitude of spheres with a radius $2R$.

Hayter and Penfold [23] received for charged, screened spheres at high volume fractions ($\mu \geq 0.2$) and moderate polyion-polyion interactions ($0.1 \leq 2R \cdot \kappa \leq 6$)

$$a(s, c) = \frac{1}{1 - 24\mu \cdot a^*(s, R, \mu, \psi_0, \kappa)} , \quad (11)$$

where a^* is a function of particle radius R, of the surface potential ψ_0 and of the Debye-Hückel inverse screening length κ. μ is defined by

$$\mu = \frac{4\pi}{3} R^3[\mathrm{nm}^3] \cdot \frac{N_L}{M} \cdot c[\mathrm{mg/ml}] \cdot 10^{-24} , \quad (12)$$

where N_L is Loschmidt's number and M is molecular mass. For strong, charge-coupled interactions of the macroions (small ionic-strength of the counter-ions) and low polymer concentrations ($\mu < 10^{-3}$), the main part of the repulsive Coulomb potential has been replaced by hard sphere impenetrability in the calculation procedure for $a(s, c)$, leading to a rescaled structure factor in the mean spherical approximation [24]. Whereas the theoretical calculation of the interaction structure factor $a(s, c)$ needs to have some prerequisite conditions met for particle dimensions, concentration, charges, and charge compensation, the solution structure factor can be estimated without such prerequisite conditions from the experimental scattering curves. A comparison with the theoretical $a(s, c)$ can be used to confirm the type of the potential, and to determine its free parameters. Furthermore, from the experimental interaction term it follows for the so-called direct correlation function [26]:

$$c^*(r, c) = \frac{10^{24} M}{2\pi^2 c N_L} \int_0^\infty s^2 \left[\frac{a(s, c) - 1}{a(s, c)} \right] \frac{\sin sr}{sr} \, ds \quad (13)$$

(c in mg/ml, s in nm^{-1}, r in nm), and for the total correlation function holds

$$h(r, c) = \frac{10^{24} M}{2\pi^2 c N_L} \int_0^\infty s^2 [a(s, c) - 1] \frac{\sin sr}{sr} \, ds . \quad (14)$$

From the latter the pair distribution function can be calculated by

$$g(r, c) = h(r, c) + 1 . \quad (15)$$

The term $4\pi r^2 g(r, c)\, dr$ describes the probability of finding a particle center within the distance interval $(r, r + dr)$ from another center, and the integral

$$N(r_1, r_2, c) = \int_{r_1}^{r_2} 4\pi r^2 g(r, c)\, dr \quad (16)$$

is the number of particles in a spherical shell with the inner and outer radii r_1 and r_2, respectively.

In Eqs. 10–16 the solution structure organization can be described, but the calculation of $h(r, c)$ is not without its difficulties [27]. The restriction

of the measurement is particularly prone to causing errors. So, the correlation functions can be discussed only tentatively and it is more advantageous when comparing samples under different environmental conditions.

Results and discussion

Shape determination

The scattering curves of CAA-nanoparticles dissolved in double distilled water are drawn in Fig. 1 for different polymer concentrations. The curves are not corrected for slit length and width smearing effects caused by the diffractometer geometry. The concentration and potential-effects are visible in the innermost part of the curves, but only weak crossing over can be detected for the scattered intensity of the highest particle concentration of 39.5 mg/ml with the low-concentration curves (about at $s = 0.06\ \mathrm{nm}^{-1}$). The solution is, as expected, free of aggregates from known negative charges at the particle surface [9] and the low-ionic strength condition of the solvent.

The scattering curves of CAA-nanoparticles dissolved in 0.15 M NaCl-solution are shown in Fig. 2. The interparticle scattering is weaker than under low-ionic conditions because of shielding of the charges at the nanoparticle surface. Aggregates exist now which can be seen in the innermost part of the scattering curves. These aggregates are larger than dimers ($R_{G,\mathrm{app}} \approx 400$ nm) and their scattering contribution can be removed by the so-called sampling-extrapolation, which has been recently described by Müller et al. [28]. The inset in Fig. 2 confirms the accomplishment of the preconditions of this method, namely, that a plateau in the $J(0)$-plot must exist. By this method, the zero-angle scattering is calculated using all other measured data at the sampling points except the zero-angle value, and this procedure is repeated for increasing step widths Δs. The plateau in the resulting curve proves the independence of $J(0)$

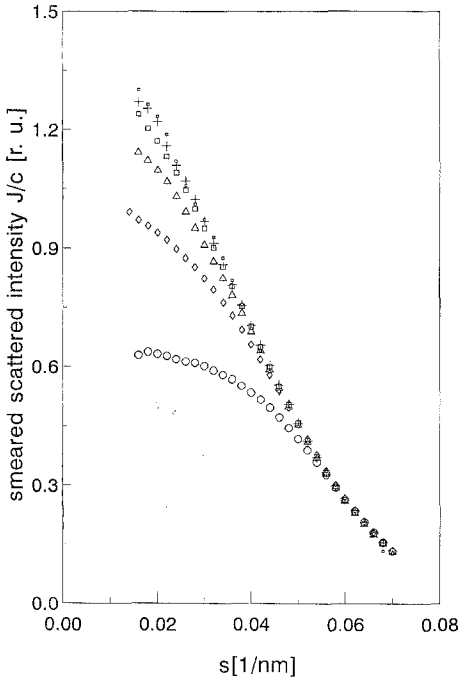

Fig. 1. Experimental uncorrected scattering curves of CAA-nanoparticles normalized to the polymer concentration: □, 1.36 mg/ml; +, 2.25 mg/ml; □, 4.65 mg/ml; △, 8.89 mg/ml; ◇, 17.9 mg/ml; ○, 39.5 mg/ml. The solvent is double-distilled water

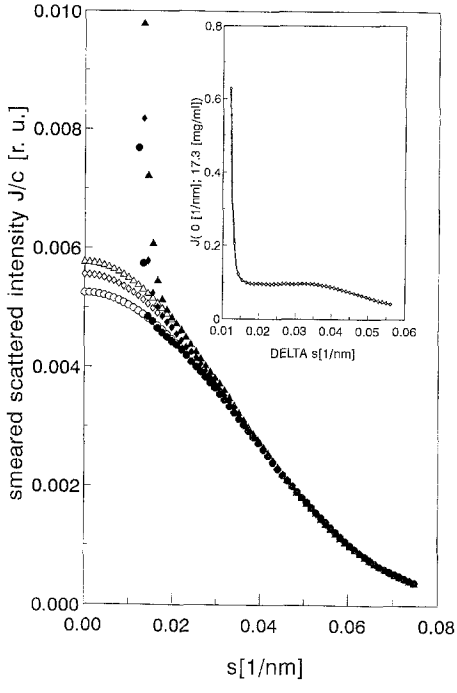

Fig. 2. Experimental uncorrected scattering curves of CAA-nanoparticles normalized to the polymer concentration: ▲, 8.57 mg/ml; ◆, 17.3 mg/ml; ●, 34.5 mg/ml. The gray-shadowed points result from sampling extrapolation to aggregate-free solutions. The solvent is 0.15 M NaCl-solution. Inset: Sampling-extrapolated zero-angle scattered intensity for selection of the optimum extrapolation step-width Δs

from the step-width. From the minimum step-width in the plateau itself, a measure π/s can be made which estimates the largest particle diameter for which information is included in the scattering at the large angle side of the first experimental point $1 \cdot \Delta s$. Taking $\Delta s = 0.022\ \mathrm{nm}^{-1}$, all scattering contributions of particles with diameters larger than 145 nm have been removed. The mass percentage of the aggregates is about 0.5% of the sample. This is in agreement with zeta potential-measurements of CAA-particles [29] which has detected a large coalescence at an ionic strength of 0.3 mol/l. Because of the low percentage of aggregates the particles could be used under physiological conditions for drug delivery systems.

The result of the correction is shown in Fig. 2 for the slit smeared curves.

From PCS-measurements it is known that the particles show a small polydispersity in their diameters. In such cases, shape determination and estimation of the diameter distribution function from only the small-angle x-ray scattering (SAXS) data is extremely difficult. Therefore, we start the discussion with the simplest shape model – with a sphere.

After a slit width-desmearing with Stokes' deconvolution method [30], the apparent radius of gyration was calculated directly from the slit length smeared curves using the Guinier-approximation for each concentration (Fig. 3). The value for infinite dilution was determined by a weighted least square fit (taking into account only data for $c = 1.36$–8.9 mg/ml for particles dispersed in water). As shown by Damaschun and Pürschel [31], the apparent radius of gyration is defined by

$$R_{G,app} = (3 \cdot V\bar{a}/8f_c)^{1/2}\ , \tag{17}$$

where $\bar{a}$ is mean electron distance and f_c is characteristic area, and, assuming monodisperse spheres, their radius can be calculated from

$$R = 1.247 \cdot R_{G,app}\ . \tag{18}$$

The resulting radii of spheres are 48.6 nm and 48.8 nm for the nanoparticles solved in water and in 0.15 M NaCl-solution, respectively. For polydisperse spheres, these values are complicatedly weighted mean values and can be used as a proof for similarity of distributions in both samples.

The complete desmearing of both series by direct methods [12] is followed by an extrapolation of the scattering curves to zero concentration via a Zimm- and Fournet-plot [14]. Because of nonlinearities in the plot for higher concentrations, under low ionic conditions only the scattering curves for $c = 1.36$–8.9 mg/ml were taken into account. The result, the pin-hole scattering curve of infinite diluted nanoparticles in water, is drawn in Fig. 4. The corresponding curve for nanoparticles dispersed in 0.15 M NaCl-solution is shown in Fig. 5.

The global form of the scattering curves of both series is very similar. The small modulation of the maxima in the scattering curve for nanoparticles dispersed in water, with an amplitude of about the diameter of the squares in Fig. 4, is caused by the desmearing procedure, rather than by real structure. But the underlying maxima and minima are not caused by the numerical data handling, they exist in the smeared scattering curves, too.

Geometrical structure parameters of the nanoparticles calculated from the scattered intensity and from the distance distribution function $p(r)$ [32] are summarized in Table 1. For unique molecular systems the radii of a sphere derived therefrom have to be identical within the experimental error limits. For a polydisperse system the geometrical structure parameters are differently weighted mean values and the mean radii derived therefrom follows the rule

$$\overline{R_n} < \overline{R_w} < \overline{R_z} < \overline{R_{max}} \tag{19}$$

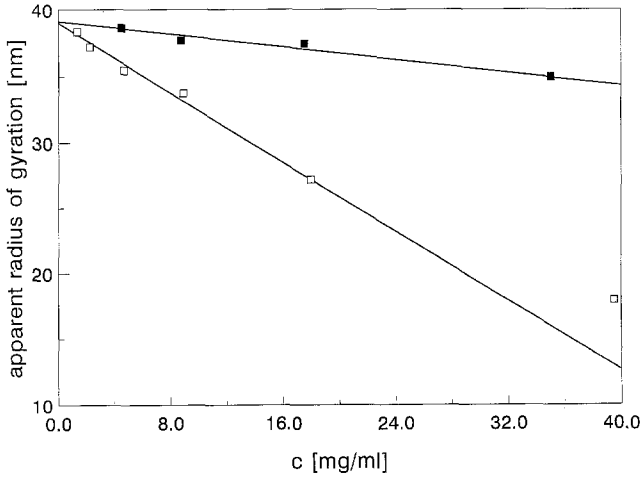

Fig. 3. Apparent radius of gyration of the CAA-nanoparticles calculated from the slit-width corrected scattering curves: □, CAA-nanoparticles in double-distilled water; ■, the solvent is 0.15 M NaCl-solution

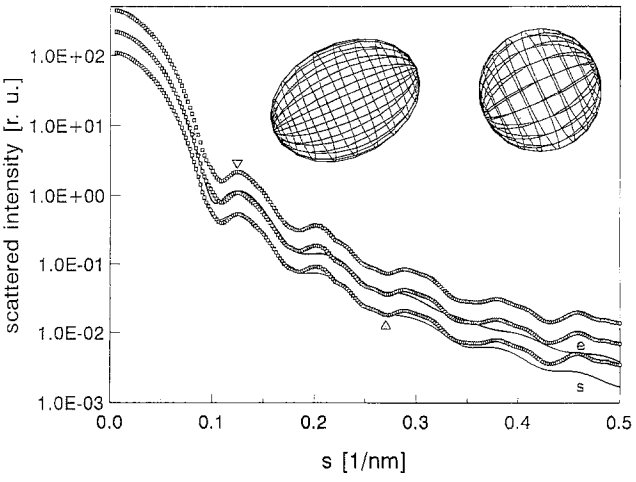

Fig. 4. Slit-corrected scattered intensity of the CAA-nanoparticles for infinite dilution in double-distilled water and comparison with model scattering curves: □, experimental data; *e* (solid line), scattering of the ellipsoid $A = 57.2$ nm, $B = 44.6$ nm, $C = 37.8$ nm (left-inset); *s* (solid line), scattered intensity of a sphere population with the distribution shown in Fig. 7 (right inset is a sphere with the radius of 45 nm). ▽, position of the first subsidiary maximum; △, inner cutoff for the fractal scattering region

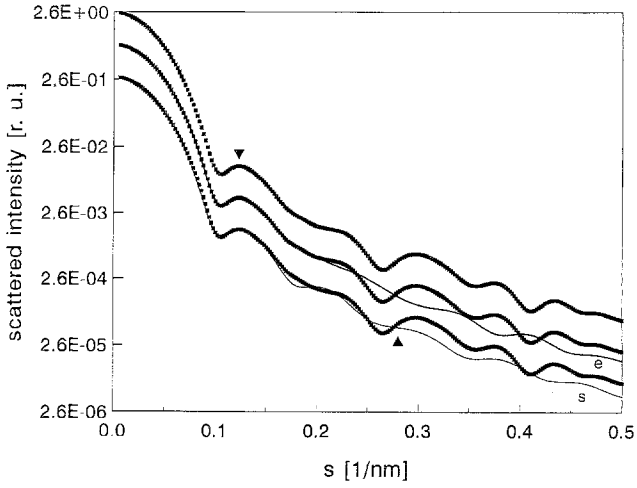

Fig. 5. Slit-corrected scattered intensity of CAA-nanoparticles for infinite dilution in 0.15 M sodium chloride and comparison with model scattering curves: ■, experimental data; *e* (solid line), scattering of the ellipsoid $A = 55.4$ nm, $B = 46.0$ nm, $C = 35.7$ nm; *s* (full line), scattered intensity of a sphere population with the distribution shown in Fig. 7. ▼, position of the first subsidiary maximum; ▲, inner cutoff for the fractal scattering region

Table 1. Structure parameters of CAA-nanoparticles solved in distilled water or in 0.15 M NaCl-solution and mean values of radii for a population of spherical molecules

		Structure parameters				Mean values of sphere radii	
		water	0.15 M NaCl			water	0.15 M NaCl
$R_{G,app}$	[nm]	39.0 ± 1	39.1 ± 1	R	[nm]	48.6 ± 1.3	48.8 ± 1.3
R_G	[nm]	38.7 ± 1	37.7 ± 1	$\overline{R_z}$	[nm]	50.0 ± 1.3	48.7 ± 1.3
L	[nm]	130 ± 5	136 ± 7	$\overline{R_{max}}$	[nm]	65.0 ± 2.5	68.0 ± 3.5
V_W	[nm^3]	(3.75 ± 0.3)·10^5	(3.84 ± 0.3)·10^5	$\overline{R_w}$	[nm]	44.7 ± 1.3	45.1 ± 1.5
				R_{smax}	[nm]	46.1 ± 0.5	47.2 ± 0.5
				R_{xmax}	[nm]	44.8 ± 0.5	44.3 ± 0.5

$R_{G,app}$-apparent radius of gyration;
R_G-*z*-averaged radius of gyration;
L-diameter of the largest particle population;
V_W-weight averaged of shape volume;
R-radius of monodisperse spheres;
$\overline{R_z}$-*z*-average of radii;
$\overline{R_{max}}$-maximum average of radii;
$\overline{R_w}$-weight average of radii;
R_{smax}-radius determined by the first subsidary maximum in the scattering curve;
R_{xmax}-radius determined by the maximum position r_{max} in the $p(r)$-function.

for the number, weight-, *z*-average- and maximum of radii. In that context, the mean value of the radius derived from the *z*-averaged radius of gyration R_G is about 10% larger than the value derived from the weight averaged shape volume V_w for particles dispersed in water as well as in 0.15 M NaCl-solution.

The type of averaging is not so clearly defined when interpreting the positions of secondary maxima in the scattered intensity (Figs. 4, 5) or the

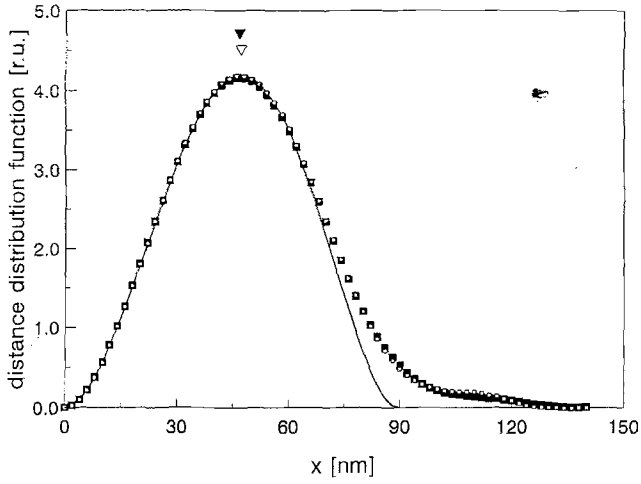

Fig. 6. Distance distribution function $p(r)$ of the CAA-nanoparticles: □, dissolved in double-distilled water; ■, dissolved in 0.15 M NaCl-solution. ▽, ▼, mark the positions of the maxima which correspond to sphere-radii of 44.8 nm and 44.3 nm, respectively. —, distance distribution of a sphere with radius $R = 44.5$ nm

location of the maximum in the distance distribution function $p(r)$ (Fig. 6) in terms of a sphere radius.

The main features in the scattering curves of both series show that the distribution of particle radii is narrow. Because the position s_{maxi} of the first subsidiary maximum in the scattering curve should only be slightly modified as well by the distribution of radii as by interparticle interferences, one can check the value for the radius of a spherical particle by using

$$R_{s\,max} = \left(2\pi - \frac{3}{2\pi}\right) \Big/ s_{maxi} \qquad (20)$$

[20]. The values of 46.1 nm and 47.2 nm in sodium chloride are somewhat larger than the weight averages, determined from the shape volume (44.7 and 45.1 nm, respectively) and from the maximum position r_{max} in the $p(r)$-function (Fig. 6) using

$$R_{x\,max} = r_{max}/1.05\,, \qquad (21)$$

which are 44.8 nm and 44.3 nm, respectively. The tail in the $p(r)$-function from 90 to 130 nm hints at the polydispersity of the samples. The large particles producing this tail stamp the z-average of the radii.

The largest diameter L represents the largest particle population, and the radii of spheres derived from it are $\overline{R_{max}} = 65$ nm and 68 nm for water and for the NaCl-solution, respectively. For comparison, Fig. 6 shows the difference between the experimental $p(r)$-function and the distance distribution of a sphere with the radius $R = 44.5$ nm.

The explanation of the different values of the radius and of the tail in the distance distribution by monodisperse elongated particles or core-shell-models failed. By two-phase-spheres (core-shell-models) the experimental scattering curves could not be simulated. The best non-linear weighted fit of the experimental scattering curve was received for a triaxial ellipsoid with the half-axes $A = 57.2$ nm, $B = 44.6$ nm and $C = 37.8$ nm (Fig. 4). The surface of the ellipsoid is $2.7 \cdot 10^4$ nm^2 and the volume $4.05 \cdot 10^5$ nm^3 is in agreement with the experimental value (Table 1). The radius of gyration of 36.6 nm is only about 5% smaller than the experimental value. But, whereas the main maximum and the first subsidiary maximum of the scattering curve are fitted within the experimental errors, the positions of the third and higher subsidiary maxima in the model scattering curve differ from those in the experimental one. For CAA-nanoparticles dissolved in 0.15 M NaCl-solution the scattering curve of a somewhat smaller ellipsoid with the half-axes 55.4 : 46.0 : 35.7 nm agrees with the experimental data up to the second subsidiary maximum. But the positions of the further extrema in model and experimental scattering curves differ significantly, too. Because of that and with the finding of a certain polydispersity by PCS [9], the monodisperse models are rejected.

Particle size distribution

To explain the long-distance tail in the $p(r)$-function a diameter distribution function for a polydisperse system of spheres has been calculated straight forwardly by Eqs. (1–5) from the scattered intensity of the CAA-nanoparticles dissolved in distilled water. The volume weighted distribution is drawn in Fig. 7. The function is at least tripartitioned, with moieties at about 64.5 nm, 90 nm, and 112 nm. The measure of polydispersity, the weight average of the volumes

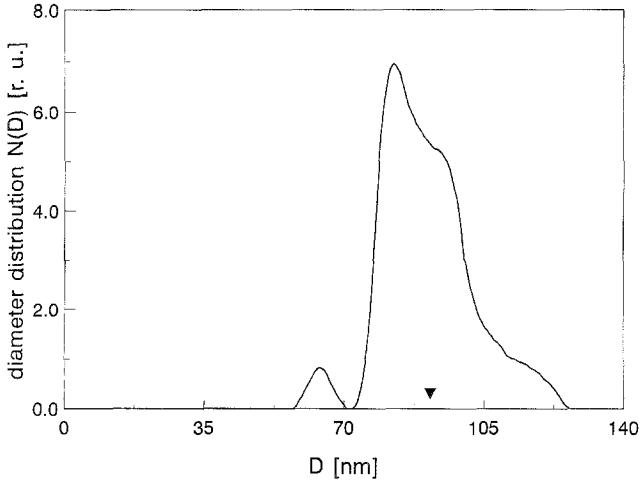

Fig. 7. Weighted diameter distribution of CAA-nanoparticles dissolved in double distilled water and in 0.15 M NaCl-solution: ▼, weighted diameter 91.8 nm

divided by their number average V_W/V_N equals 1.16. From the number average $V_N = 3.52 \cdot 10^5$ nm^3 a mean radius of the spheres of 43.8 nm, and from the weight average $V_W = 4.06 \cdot 10^5$ nm^3 a mean value of 45.9 nm has been calculated. The z-average of the radius of gyration has been calculated from the distribution to 37.8 nm. That means both the z-average and the weight average of the radii of the sphere distribution agree with the experimental values within the error limits.

The reconstitution of the scattered intensity by Eq. (6) from the scattering of spheres with a diameter distribution corresponding to Fig. 7, which was sampled in steps of $\Delta x = 0.5$ nm, provides a curve which also fits the experimental values within the experimental error level (Fig. 4). For water-dissolved particles, especially the positions of the subsidiary maxima are identical in both the experimental and reconstituted curves. From that it follows that the nanoparticles in water are mainly represented by a sphere population with radii of about 45–46 nm.

In the case of CAA-particles dissolved in 0.15 M sodium chloride, the particle size distribution is nearly identical to the former one, although the second subsidiary maximum in the scattering curve (Fig. 5) is not fitted very well after reconstitution.

Surface roughness

Both model scattering curves, as well for ellipsoids as for a system of polydisperse spheres, deviate from the experimental data at larger scattering vectors (Figs. 4, 5). The deviation is significant and cannot be caused by a wrong background subtraction during the handling of the experimental data, as has been proved. The experimental scattered intensity decreases slower than model data, indicating some inner structure of the particles or a fractal behavior.

By a least square method the scattering was fitted to a power law in the region between $s_{min} = 0.222$ nm^{-1} and $s_{max} = 0.41$ nm^{-1} (Fig. 8).

Over more than two decades the scattered intensity declines as

$$I(s) = \text{const.}/s^{3.647} . \tag{22}$$

With the exponent 3.67 ± 0.1 a scattering behavior like a mass fractal can be excluded, because its scattering behaves as

$$I(s) = \text{const.}/s^{D} , \tag{23}$$

and the fractal dimension D must be less than 3.

A surface fractal scatters like

$$I(s) = \text{const.}/s^{6-D} \tag{24}$$

[33], that means D equals 2.3 ± 0.1. That is a value which characterizes a rather smooth surface. The self-similarity of the fractal is restricted to a length scale of $\pi/s_{min} > r > \pi/s_{max}$. This region is not sharply defined in the scattering curve. Taking the lower cutoff-value for the fitting interval 0.222 nm^{-1} as an estimate of s_{min}, the outer cutoff r_{max} will be 14 nm. Choosing the visible point of divergence (Figs. 4, 5) between the experimental and reconstituted scattering curve at 0.275 nm^{-1} the value is 11.4 nm for the outer cutoff of the scale. The inner cutoff r_{min} may correspond to atomic length. It cannot be determined exactly, because of the restricted experimentally scanned angular region.

An upper limit of 7.7 nm is given by the fitting interval boundary $s_{max} = 0.41$ nm^{-1}. With these cutoffs the condition [34]

$$r_{max}/r_{min} > 2^{1/D} \tag{25}$$

is fulfilled and the experimental value $D = 2.3 \pm 0.1$ can be accepted as a well defined dimension. That means the value of 53 m^2/g polymer for the specific surface of a smooth spherical nanoparticle is enlarged for interacting reagents smaller than 11.4 nm in diameter. The fractal properties of particles in both solutions are identical. From this

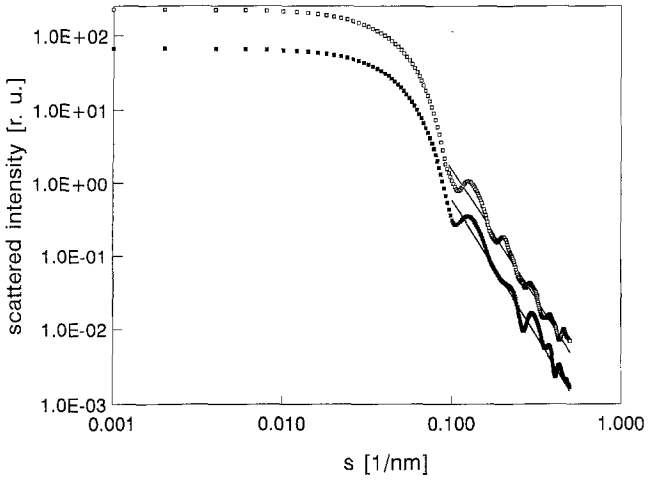

Fig. 8. Surface fractality of the CAA-nanoparticles dissolved in low and physiological ionic strength media; □, experimental scattered intensity in double distilled water; ■, experimental scattered intensity in 0.15 M NaCl-solution. Straight lines follows the law const/$s^{3.67}$, i.e., fractal dimension $D = 2.3$

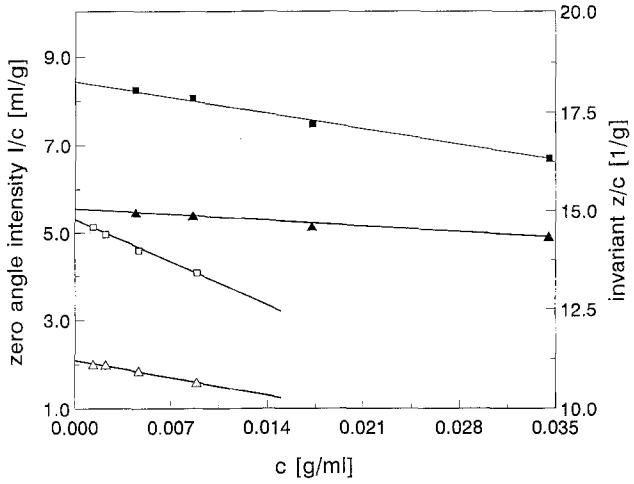

Fig. 9. Concentration dependence of reduced zero-angle scattered intensity and invariant for determination of molecular masses without absolute measurement: □, I/c in double-distilled water (to multiply by 1000); ■, I/c in 0.15 M NaCl-solution (to multiply by 100); △, invariant z/c in double-distilled water (to multiply by 10^{18}); ▲, invariant z/c in 0.15 M NaCl-solution (to multiply by 10^{17})

it can be concluded that charges should not provoke a changed surface roughness (at the reached structure resolution) in the case of CAA-nanoparticles.

Molecular mass and hydration

The molecular mass of the nanoparticles in both solutions has been calculated from Eqs. (7) and (8). The extrapolation of the zero-angle scattered intensity to zero concentration is shown in Fig. 9, and the value $(I(0)/c)_{c=0}$ was calculated by a least square procedure to be 844 ml/g for particles in 0.15 M NaCl-solution.

The first derivative of the reduced invariant z/c is $dz/dc = -2.2 \cdot 10^{15}$/g. From that the weighted molecular mass is determined to be $2.31 \cdot 10^8$ g/mol. For a comparison of the experimental and of the dry volume calculated via

$$V_{dry} = \frac{M \cdot \bar{v}}{N_L} \cdot 10^{21} \, [nm^3] \,, \tag{26}$$

the partial specific volume must be measured. Using the densitometer DDA 02 (A. Paar-KG., Graz), we measured $\bar{v} = 0.81$ cm^3/g, and the dry volume is then $V_{dry} = 3 \cdot 10^5$ nm^3. In general, the hydration of a particle cannot be determined exactly from small-angle x-ray scattering alone [35]. The numerical value

$$w = \bar{v}d(V/V_{dry} - 1) \tag{27}$$

where d is mass density of the solvent and V is molecular volume of the particle in solution is falsified when using poorly resolved scattering curves. Here, we reached a resolution of about $\pi/s_{max,exp} = 6$ nm. With $V_W = 3.8 \cdot 10^5$ nm^3 we got 0.22 g water per g polymer, a value which should mainly reflect the resolution effects. A value of 0.22 g/g is of the same order of magnitude or smaller than determined by Eq. (27) for globular proteins [36]. That means, in analogy to the proteins, that there are no such large cavities inside the CAA-nanoparticles, as discussed for polycyanoacrylate-nanoparticles by Kreuter [7] and for styrenecopolymers by Cheng et al. [37]. The fictive "hydration" of 0.22 g/g is in agreement with the roughness (fractality) of the surface as described above.

The same procedure has been used to determine the molecular mass for CAA-nanoparticles dissolved in distilled water. For small concentrations, $c < 0.010$ g/ml, the linearity of the reduced zero-angle intensity $I(0)/c$ and of the reduced invariant z/c with the concentration is maintained (Fig. 9). The molecular mass has been calculated using Eqs. (7) and (8) with the extrapolated values

$[I(0)/c]_{c=0} = 5312$ ml/g and $dz/dc = -64.44 \cdot 10^{18}$ l/g to $4.965 \cdot 10^7$ g/mol. The large discrepancy of the value found for screened particles in sodium chloride is caused by ordering effects other than hard sphere or van der Waals interactions. It was shown formerly [9] that the CAA-nanoparticles are negatively charged, and so Coulombic repulsive forces should act between the particles. The strict usage of Eqs. (7) and (8) fails under these conditions where unscreened charged particles exist in the solution, but for concentrations smaller than 0.01 g/ml the measured interference effects are proportional to the physical concentration in the measurable angular region. That can be concluded from the Zimm- and Fournet-plots. For the determination of the scattering curves with infinite dilution of CAA-particles the relative value of the concentration for each sample is sufficient, but for the molecular mass a determination of the absolute value is necessary. That means the Zimm- and Fournet-plots are successful for particles dissolved in water, because the reduced scattered intensity $I(s)/c$ has only to be proportional to concentration.

Whereas Hansen and Hayter [24] used in their theory of rescaled potentials for highly diluted, screened, charged spheres larger hard sphere-cores and a fixed particle concentration to simulate Coulombic potential effects, we replace in a first approximation the Coulomb potential by hard spheres with Lennard-Jones potentials (Fournet-approximation) and take a higher effective concentration into account. That means the Fournet-formula (10) for the solution structure factor $a(s, c)$ is used. By a curve-fitting procedure an effective volume fraction μ has been estimated for each experimentally determined solution structure factor (Fig. 10). Taking the apparent molecular mass of $5 \cdot 10^7$ g/mol into consideration and using Eq. (12), one receives from the linear part in the inset of Fig. 10 an effective concentration 4.7 times larger than the real physical concentration. With this scaling factor and the enlarged effective concentration the molecular mass of nanoparticles in distilled water is $2.33 \cdot 10^8$ g/mol (Eqs. (7) and (8)). In that way, the molecular masses of the nanoparticles under low and moderate (0.15 M NaCl-solution) ionic conditions have been determined completely independently from each other. They are identical within the error limits of about 10%. From that it follows that all conclusions concerning the hydration and inner structure of the CAA-particles hold for both ionic conditions.

Order of nanoparticles in solution

The interparticular interference effects, visible in the scattering curves of particles (Figs. 1, 10) dispersed either in water or in 0.15 M NaCl-solution, renders possible a structural characterization of the solution. Independent of the kind of interactions, of existing short-range or long-range potentials, the direct and total correlation functions can be calculated from Eqs. (13, 14). Figures 11 and 12 show the curves for the highest particle concentrations 39.5 mg/ml and 34.5 mg/ml if the nanoparticles are immersed in water or in 0.15 M NaCl-solution, respectively.

The difference between the direct and total correlation functions of the nanoparticles in NaCl-solution is small, because of shielding the negative charges at the particle surface by sodium counter-ions. The Debye-Hückel radius is about 0.8 nm for the ionic condition used, that means the particles should interact nearly as independent hard spheres via a short range potential. This is confirmed by the pair distribution function

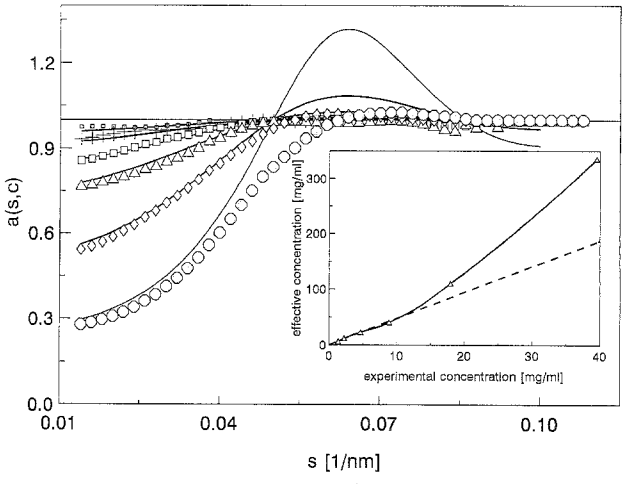

Fig. 10. Comparison of experimental and model solution structure factors for CAA-nanoparticles dissolved in double-distilled water: □, 1.36 mg/ml; +, 2.25 mg/ml; □, 4.65 mg/ml; △, 8.89 mg/ml; ◇, 17.9 mg/ml; ○, 39.5 mg/ml. Solid lines: Fournet-model fitting using the apparent molecular mass of $5 \cdot 10^7$ g/mol and the effective concentrations are shown in the inset

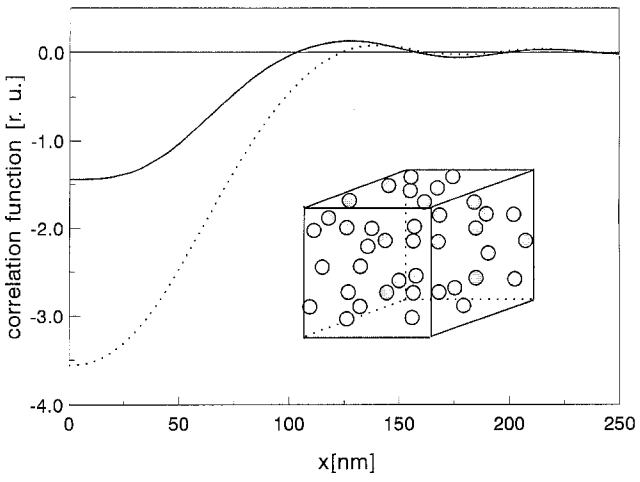

Fig. 11. Direct and total correlation function of CAA-nanoparticles dissolved in double distilled water: . . . , direct correlation function; — total correlation function. Inset: nanoparticle order in solution with local decomposition

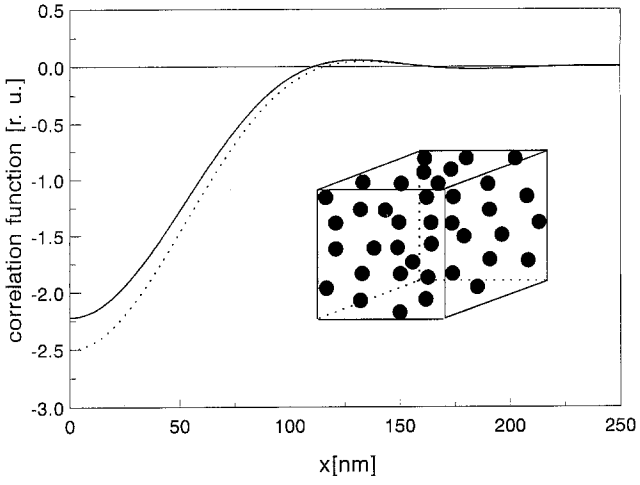

Fig. 12. Direct and total correlation function of CAA-nanoparticles dissolved in 0.15 M NaCl-solution . . . , direct correlation function; — total correlation function. Inset: random order of nanoparticles in solution

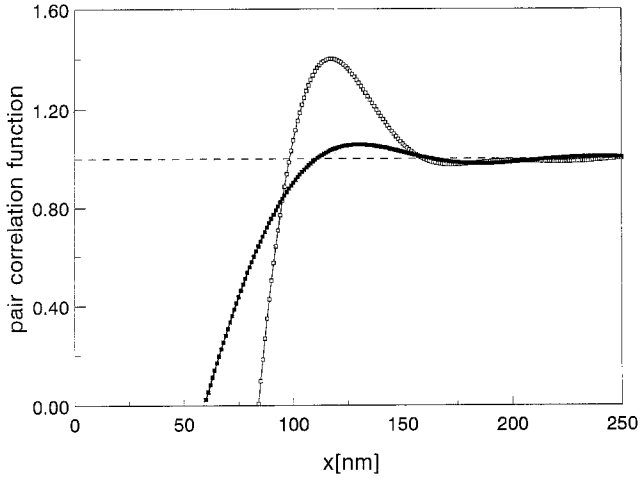

Fig. 13. Pair correlation function of CAA-nanoparticles in moderate concentrated solutions: □, double distilled water, $c = 39.5$ mg/ml; ■, 0.15 M NaCl-solution, $c = 34.5$ mg/ml

(Fig. 13) which has been calculated by Eq. (15). The shielded particles have only an excluded-volume region and $g(r)$ rapidly approach unity, i.e., the particle positions are not correlated over large distances. The solution shows a random order of hard spheres. The next-neighbor number in a shell between 110 and 160 nm, calculated from the radial distribution function corresponding to Eq. (16) is 1.2. This value agrees with a statistical random distribution, as can be deduced from the volume concentration of $\mu = 0.0367$. The non-zero values of the pair distribution for distances between 65 and 95 nm may be caused by the existing small polydispersity of the sample which also contains particles of 65 nm in diameter.

If the nanoparticles are dispersed in the medium with low ionic strength, the interaction is changed completely. Figure 11 shows the large discrepancy between direct and total correlation functions, which manifests itself in the multiple long-range interactions between the unshielded charged nanoparticles. In the case of overall repulsive interactions the particles tend to diffuse as far as possible from each other without finding a stable order. The distance between next neighbors in a cubic-face-centered structure would be about 260 nm. Here, the pair distribution $g(r)$ shows a larger volume-excluded region caused by the repulsive potentials as for the shielded particles, but a weak term of attractive forces exists, because the maximum in $g(r)$ indicates a certain degree of short-range order. The number of next neighbors is 1.8 in a shell between 104 and 158 nm. That is 0.5 particle more than in the case of random distribution. It remains to be mentioned that in the case of non-shielded negatively charged particles the distances around 200–250 nm are essential for discussion of long-range order effects. The cutoff of the measurable small-angle region at $s = 0.012\ \mathrm{nm}^{-1}$ corresponds

to a region of $x < 260$ nm, so there are uncertainties when discussing large distances > 200 nm.

In the framework of the DLVO-theory (Derjaguin-Landau-Verwey-Overbeek) the solution structure factor $a(s, c)$ can be calculated for a sum of repulsive screened Coulombic interactions and attractive van der Waals forces (DLVO-theory) [38]. But attractive potentials may exist also for pure Coulombic interaction between equally named charges, if counter-ions are included [39]. Common counter-ions between equally charged nanoparticles may cause local decompositions and preferential neighborhoods of macromolecules.

The mean spherical approximation and the rescaled mean spherical approximation, which are based on a Vervey-Overbeek potential [23, 24], can be used under certain restrictions for the diameters of the spheres, the Debye-Hückel screening length, volume fraction and surface charges. For the particles under investigation, the restrictions are not sufficiently fulfilled and a modeling will follow elsewhere in connection with the studies of effects of surfactants and adjuvants on the order of the CAA-nanoparticles under defined ionic surroundings.

Conclusions

The investigation of the synthetic nanoparticles by small-angle x-ray scattering provides structural information in a direct way.

In general, the determination of the shape form factor in charged polydisperse polymeric systems is a crucial point. But, because the particle parameters were estimated from two complete sets of experimental scattering curves for different ionic conditions and a model was found without contradictions, the charge and excluded-volume influences on the scattering curve should be eliminated correctly. The method for determination of the molecular mass without absolute intensity measurement is a convenient procedure for charged systems, too, if the potential effects are linear with the concentration and when taking into account the effective volume concentration of the polymer. The value of $2.3 \cdot 10^8$ g/mol is confirmed by hydrodynamic measurements, as will be discussed in a separate paper. The CAA-nanoparticles exist as a population of spheres with a relatively narrow diameter distribution (polydispersity index $R_w/R_N = 1.05$) with two minor subpopulations at radii of 32 nm and 66 nm and a main component at 45 nm. This means that the polydispersity corresponds to the value measured by photon correlation spectroscopy (PCS) [9], which involves fitting of the measured multicorelation function by a weighted sum of model exponential functions. The radii of the main component spheres are very similar for SAXS and PCS, if the corresponding z-averages are compared. The somewhat enlarged values measured with PCS may result from a shell of H_2O diffusing together with the nanoparticles. The existing subpopulations have different surface/volume quotients and will show different hydrophobic areas for a given volume percentage of acrylic acid. Indeed, by hydrophobic interaction chromatography [9] a corresponding retarded elution of several fractions is observable. Because the fractions possibly interact with different blood components in vivo, this may lead to variations in their organ distribution and to differences in their clearance velocity.

The difference between the particle dry volume of $3.0 \cdot 10^5$ nm^3 and the particle model volume of $4 \cdot 10^5$ nm^3 is in the limit which can be expected from the structure-resolution effects discussed by Müller et al. [35], and is in agreement with a rather tightly packed nanoparticle structure without inner cavities. From this it can be concluded that loading of the CAA-nanoparticles with drugs should be realized mainly by the adsorption of drugs on the outside of the particles and an entrapment in inner pores is excluded. Because of the detection of a certain surface structure by Dittgen et al. [40] using transmission electronmicroscopy, the deviation of the scattering curve-tail at larger angles from a $1/s^4$-law should be discussed in terms of a certain fractality of the surface rather than by inner electron density fluctuations. The fractal dimension $D = 2.3$ enhances the real surface for probe-particles with diameters less than 11.4 nm, when comparing with the specific surface of 53 m^2/g calculated from the smooth spherical model. Larger reagents will feel the nanoparticles to be smooth. D is useful especially in comparative studies [41]. It affects the diffusion of reagents on the surface of nanoparticles, determines rate and position of arrival of surfactants [42], and resembles an estimation of the monolayer capacity for adsorptive

bound molecules, because this number is proportional to d^D, d being the diameter of the adsorbed molecule. The surface fractal distance of 11.4 nm is in agreement with the dimension of a region named "swollen shell" found by electronmicroscopy [40]. It has been discussed by Tamai et al. [43] and Shirahama and Suzawa [44] that this shell should be built up from hydrophilic chains. In our case they are carrying COOH-groups. These chains influence the adsorption of blood components.

For water as well as for 0.15 M sodium chloride solutions, the structural parameters of the CAA-particles are not influenced significantly by the surrounding counter-ions. In physiological sodium chloride there is a small percentage of aggregates with diameters about 10 times as large as the monomers. These particles will behave differently than the monomers in vivo. They will be recognized by macrophages and cleared by RES first, but because of the low percentage they will not influence the suitability of the nanoparticle population for drug delivery purposes.

The interaction behavior of the negatively charged nanoparticles at physiological ionic strengths is in agreement with the in vivo observation of an increased binding and RES clearance for charged particles (for review see [6]). The surface charges are screened by counter-ions and hamper the particle cell interactions at short distances only. Therefore, the electrostatic repulsive interactions between the negatively charged carrier and the sialic acids in the cell wall of macrophages should be negligible, and the receptor-mediated recognition and clearance of the drug carrier is possible. To avoid recognition and clearance of the drug carrier by the RES and to control the organ distribution the surface properties of the carrier has to be modified, e.g., by hydrophilic coating particles [3]. The structure of such modified nanoparticles and their interaction behavior is the next point of our investigations by small-angle x-ray scattering.

Acknowledgments

This work was supported by grants from the Deutsche Forschungsgemeinschaft (Mu 989/1-1), from the Bundesministerium für Forschung und Technologie (0310188A, 0319682A) and by a Grant from the Fonds der Chemischen Industrie to G.D.

References

1. Verdun C, Couvreur P, Vranckx H, Lenaerts V, Roland M (1986) J Controlled Release 3:205
2. Tarcha P (1991) Polymers for Controlled Drug Delivery, CRC Press, Boca Raton Ann Arbor, Boston
3. Müller RH, Davis SS, Illum L, Mak E (1986) Particle charge and surface hydrophobicity of colloidal drug carriers. In: Gregoriadis S, Senior J, Poste G (eds) Targeting of Drugs with Synthetic Systems) Plenum Press, New York, p 239
4. Van Oss CJ, Gillman CF, Neumann HW (1975) Phagocytic engulfment and cell adhesiveness as cellular surface phenomena, Marcel Dekker, New York
5. Van Oss CJ, Gillman CF, Neumann HW (1984) Ann NY Acad Sci 416:332
6. Müller RH (1991) Colloidal Carriers for Controlled Drug Delivery and Targeting-Modification, Characterization and in Vivo Distribution. Wissenschaftliche Verlagsgesellschaft. CRC Press, Stuttgart/Boca Raton
7. Kreuter J (1983) Int J Pharm 14:43
8. Pfeifer P (1987) In: Laszko P (ed) Preperative Chemistry, Academic Press, New York, p 13
9. Lukowski G, Müller RH, Müller BW, Dittgen M (1992) Int J Pharm 84(1):23
10. Ametani K, Fujita H (1978) Japanese Journal Appl Physics 17:17
11. Damaschun G, Pürschel HV (1969b) Monatshefte Chemie 100:274
12. Müller JJ (1992) In: Programmpaket APX 63, Small-Angle X-Ray Scattering, Freiberger Präzisionsmechanik GmbH, Freiberg, p 1
13. Marquardt DW (1963) J Soc appl Math 11:431
14. Glatter O, Kratky O (1982) In: Small-Angle X-ray Scattering, Academic Press, London
15. Feigin LA, Svergun DI (1987) In: Taylor GW (ed) Structure Analysis by Small-Angle X-Ray and Neutron Scattering, Plenum Press, New York
16. Walter G, Gerber T, Kranold R (1983) Studia biophysica 97:129
17. Kratky O, Pilz I, Schmitz PJ (1966) J Colloid and Interface Sci 21:24
18. Stabinger H, Kratky O (1978) Makrom Chem 179:1655
19. Plestil J, Pospisil H, Ostanevich Yu M, Degovics G (1991) J Appl Cryst 24:659
20. Guinier A, Fournet G, Walker CB, Yudowitch KL (1955) In: Small-Angle Scattering of X-Rays. John Wiley & Sons, New York
21. Enderby JE, March NH (1965) Adv in Physics 14:453
22. Palmer RG, Weeks JD (1973) J Chem Phys 10:4171
23. Hayter JB, Penfold J (1981) Molec Physics 42:109
24. Hansen JP, Hayter JB (1982) Molec Phys 46:651
25. Fournet G (1951) Acta Cryst 4:293
26. Zernicke F, Prins JA (1927) Z Physik 41:184
27. Paalman HH, Pings CJ (1962) J Appl Phys 33:2635
28. Müller JJ, Zalkova TN, Damaschun G, Misselwitz R, Serdyuk IN, Welfle H (1986) Studia biophysica 112:151
29. Lukowski G, Müller RH, Müller BW, Dittgen M (1992) Europ J Pharm and Biopharm 38(1):41
30. Stokes AR (1948) Proc Phys Soc London 61:38

31. Damaschun G, Pürschel HV (1969) Monatshefte Chemie 100:510
32. Damaschun G, Müller JJ, Pürschel HV, Sommer G (1969) Monatshefte Chemie 100:1701
33. Schmidt PW (1991) J Appl Cryst 24:414
34. Pfeifer P (1984) Appl Surf Sci 18:146
35. Müller JJ, Damaschun G, Schmidt PW (1985) J Appl Cryst 18:241
36. Damaschun G, Damaschun H, Dembo AT, Kayushina RL, Kröber R, Moshkov KA, Müller JJ, Neifakh SA, Rolbin JA, Shavlovsky MM, Zirwer D (1978) Studia biophysica 71:53
37. Cheng CM, Micale FJ, Vanderhoff JW, El-Asser MS (1992) J Colloid Interface Sci 150:549
38. Verwey EJW, Overbeek JTG (1948) Theory of the stability of lyophobic colloids, Elsevier, Amsterdam
39. Ise N (1986) Angew Chemie 98: 323
40. Dittgen M, Zosel B, Kunze H (1988) Pharmazie 43:872
41. Lukowski G, Müller RH, Müller BW, Dittgen M (1993) Colloid Polym Sci 271:100
42. Pfeifer P (1987) In: Laszko P (ed) Preparative Chemistry Academic Press, New York, p 13
43. Tamai H, Murakami T, Suzawa T (1985) J Appl Polym Sci 30:3857
44. Shirahama H, Suzawa T (1985) Colloid Polym Sci 263:141

Received July 12, 1993;
accepted October 25, 1993

Authors' addresses:

J.J. Müller
Max-Delbrück-Centre for Molecular Medicine
Robert-Rössle-Str. 10, 13122 Berlin-Buch, FRG

G. Lukowski
Department of Pharmaceutics, E.-M.-Arndt-University,
Jahnstr. 17, 17489 Greifswald, FRG